Journal of Renewable Materials

Tech Science Press

DOI: 10.32604/jrm.2022.022283

ARTICLE

Graphene-Based Active Tunable Metasurfaces for Dynamic Terahertz Absorption and Polarization Conversion

Haoran Wei, Tian Ji and Jianqing Huang*

College of Applied Science and Technology, Hainan University, Danzhou, 571737, China

*Corresponding Author: Jianqing Huang. Email: hjqoffice@163.com

Received: 24 March 2022 Accepted: 29 April 2022

ABSTRACT

Simultaneous broadband absorption and polarization conversion are crucial in many practical applications, especially in terahertz communications. Thus, actively tunable metamaterial systems can exploit the graphene-based nanomaterials derived from renewable resources because of the flexible surface conductivity and selective permeability of the nanomaterials at terahertz frequencies. In this paper, we propose a graphene-based active tunable bifunctional metasurface for dynamic terahertz absorption and polarization conversion. The graphene ring presents a certain opening angle (A) along the diagonal of the *xoy* plane. When $A = 0°$, the proposed metasurface behaves as a broadband absorber. Numerical results show the feasibility of achieving this polarization-insensitive absorber with nearly 100% absorptance, and the bandwidth of its 90% absorptance is 1.22 THz under normal incidence. Alternatively, when $A = 40°$ after optimization, the proposed metasurface serves as a broadband polarization convertor, resulting in robust broadband polarization conversion ratio (PCR) curves with a bandwidth surpassing 0.5 THz in the reflection spectrum. To tune the PCR response or the broad absorption spectrum of graphene, we change the Fermi energy of graphene dynamically from 0 to 0.9 eV. Furthermore, both the broadband absorption and the linear polarization conversion spectra of the proposed metasurface exhibit insensitivity to the incident angle, allowing large incident angles within 40° under high-performance operating conditions. To demonstrate the physical process, we present the impedance matching theory and measure electric field distributions. This architecture in the THz frequency range has several applications, such as in modulators, sensors, stealth, and optoelectronic switches. THz wave polarization and beam steering also have broad application prospects in the field of intelligent systems.

KEYWORDS

Metasurface; broadband absorption; polarization conversion; bi-functional; renewable resources

1 Introduction

The terahertz (THz) frequency range is difficult to investigate in the essential region of Electromagnetic Spectrum. The frequency range is in the 0.1–10 THz range of electromagnetic waves [1,2] and lies between the infrared and microwave bands. It is also being explored and applied gradually in many fields, such as high-speed futuristic sixth-generation wireless communication [3], three-dimensional tomography [4,5], and security imaging [6,7]. However, the efficiency of natural materials in THz radiation is low, causing considerable challenges in the research on devices with absorption, filtering, and polarization conversion

and modulation; consequently, the application and development of THz technology is limited [2,8]. "Metasurfaces" are composite materials with deliberate structures, and they exhibit supernormal physical attributes lacking in natural materials. For example, the macroscopic electromagnetic properties of a structure can be controlled by artificially designing the shape and size of the lattice unit or changing the voltage and other external factors. Thus, the rise of metasurfaces has facilitated research on high-performance, broadband THz functional devices [9–12].

In various functional meta-devices, perfect absorbers [13–17] and polarization converters [18–22] are primary components mainly used for manipulating THz waves [23–25] in several fields. Graphene carbon-based nanomaterial has a two-dimensional (2D) honeycomb structure comprising a single layer of carbon atoms. The nanomaterial exploits flexible surface conductivity and selective permeability at THz frequencies for actively tunable metamaterial systems [26]. The nanomaterial is also obtained from renewable resources, meets the current demand for sustainable advanced materials, and has high economic benefits and eco-friendliness; these advantages make the material suitable for green, high-quality, and sustainable production [27–29]. Alves et al. [15] constructed a single-band terahertz metamaterial absorber using an aluminum square periodic array and an aluminum ground plane, which were separated by a thin silica layer. The terahertz metamaterial achieved an absorption efficiency of approximately 100%. Kang et al. [16] proposed a terahertz metamaterial perfect absorber based on Dirac semimetals and vanadium dioxide (VO_2). The absorber is dual-controlled for frequency adjustment. Changing the Fermi energy of the DFS or conductivity of the VO_2 can change the resonance frequency of the absorber, which can be utilized to achieve tunability. Hu et al. [17] created a tunable broadband THz absorber using a single-layer graphene ring array with plasma hybridization. In normal incidence, the proposed design can achieve broadband absorption with more than 90% absorptance in the frequency range of 0.88–2.10 THz. The *L*-shaped metamaterials used in the THz broadening polarization converter proposed by Sun et al. [18] are a departure from previous work but have a polarization conversion efficiency greater than 80% in the frequency range of 0.64–1.19 THz. Yadav et al. [19] proposed a THz polarization converter based on the ϕ-shaped graphene metasurface in the form of an arrow; the converter is broadband adjustable. During operation in the frequency range of 5.08–6.89 THz, the converter produces a linear polarization conversion response and maintains stability throughout a wide range of incidence angles. Although the developed metasurface can flawlessly convert terahertz wave absorption and polarization, only a few studies have combined the two functionalities into a single-layer metasurface structure.

This work theoretically proposes a dynamically tunable broadband bi-functional THz metasurface based on a monolayer graphene split ring. The simulation results show that when the opening angle is set to 0°, the designed metasurface behaves as a broadband absorber. The frequency range of 0.88–2.10 THz can be effectively absorbed by this absorber in normal incidence, resulting in more than 90% effective absorption. When the opening angle is set to 40°, the proposed design can also be regarded as a broadband polarization converter; further, the design achieves a polarization conversion efficiency of more than 90% across a bandwidth of approximately 0.5 THz. Therefore, in the target THz range, the dual-function characteristics of the proposed design are sufficiently realized by switching the structural parameters. The graphene Fermi energy was varied in the simulation, and the desired amplitude of the ideal broadband absorption response of the design increased from 20% to 100%. Moreover, the peak frequency of the polarization conversion efficiency was blue-shifted from 1.05 to 1.38 THz. We demonstrated that the proposed design exhibits active adjustable properties and has a wide range of application possibilities in the field of THz communications.

2 Design and Simulation Methods

Figs. 1a and 1b illustrate the unit-cell structure of the proposed metasurface. A three-layer structure was used to construct the metasurface: a single annular graphene sheet was on top, and the intermediate dielectric barrier was composed of SiO_2 film, with a relative permittivity of 3.9 [17]. Gold with

conductivity $\sigma = 4.56 \times 10^7$ S/m was used as the bottom anti-transmission layer [30]. The optimal solutions of the cell geometry parameters obtained after parametric scanning were $R_{in} = 5$ μm, $R_{out} = 16$ μm, $p = 35$ μm, $d = 1$ μm, and $t = 25$ μm. The surface conductivity (σ_g) of graphene can be described by the Kubo formula [31]:

$$\sigma_g = \frac{ie^2 k_B T}{\pi\hbar(\omega + i\tau^{-1})}\left[\frac{\mu_c}{k_B T} + 2\ln\left(e^{-\frac{\mu_c}{k_B T}} + 1\right)\right] + \frac{ie^2}{4\pi\hbar}\ln\left[\frac{2|\mu_c| - \hbar(\omega + i\tau^{-1})}{2|\mu_c| + \hbar(\omega + i\tau^{-1})}\right], \quad (1)$$

where e is the electronic charge, k_B is the Boltzmann constant, h is the approximate Planck constant, ω is the angular frequency, τ is the relaxation time, μ_c is the Fermi energy, and $T = 300$ K is the Kelvin temperature. To calculate the electromagnetic response of the bi-functional metasurface proposed in this study, we performed numerical simulations in the THz range using the commercial software CST Microwave Studio (Computer Simulation Technology, Germany). Also, a single unit cell is meshed using a frequency-domain finite element method (FEM), and periodic boundary conditions in the x and y directions as well as open conditions in the z direction. Additionally, the monolayer graphene sheet is treated as a surface impedance layer because of its low thickness and high surface impedance. For the absorption mode ($A = 0°$), a value of 0.1 ps was specified for the initial relaxation time of graphene as well as a value of 0.9 eV for the initial Fermi energy of graphene.

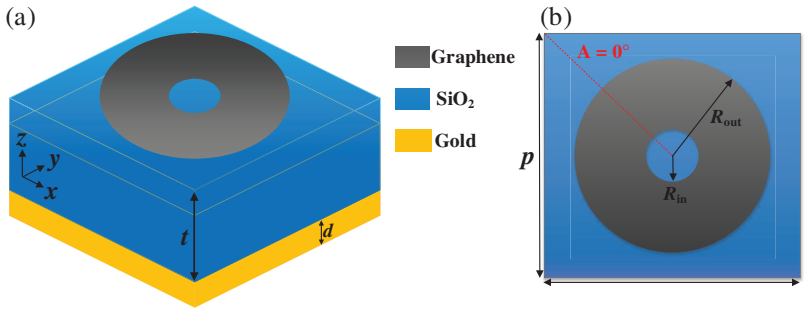

Figure 1: Schematic of the unit-cell structure of the proposed design: (a) Side view; (b) Top view

Furthermore, we incorporated metallic components as a strategy to enhance the absorption behavior of graphene. The strategy improves the working performance but reduces the chemical stability, increases preparation cost, and lowers commercialization feasibility. However, graphene preparation from bare biomass, which guarantees desirable performance [32], improves the possibility of sustainable and large-scale graphene production as well as economic benefits. Iodine cations can also be used to bridge graphene sheets to enhance the interconnection between the sheets, improving the absorption efficiency [33] and consequently the suitability for practical application under complex conditions.

3 Results and Discussions

3.1 Proposed Switchable Metasurface Behaves as a Broadband Absorber When A is Fixed at 0°

The broadband reflection, transmission, and absorption spectra of the proposed metasurface are presented in Fig. 2a when the opening angle of the top graphene ring is set at $A = 0°$. As the opening angle of the graphene ring resonator is 0°, the metasurface can be considered an anisotropic structure; thus, its absorption spectrum is polarization insensitive to the different polarization angles. Taking the graphene sheet with the Fermi energy of 0.9 eV as an example, the reflectance $R(\omega)$, transmittance $T(\omega)$, and absorbance $A(\omega)$ depend on the frequency-dependent S-parameters and are calculated as follows [34]:

$$\begin{cases} R(\omega) = |S_{11}(\omega)|^2 \\ T(\omega) = |S_{21}(\omega)|^2 \\ A(\omega) = 1 - R(\omega) - T(\omega) \end{cases} \tag{2}$$

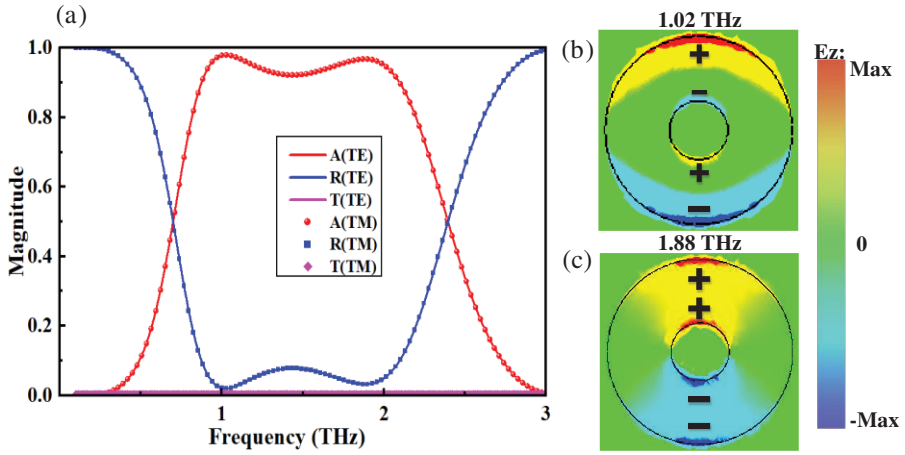

Figure 2: (a) Reflection, transmission, and absorption spectra of the proposed metasurface in different polarization modes; *z*-component distributions of the electric field of the graphene layer at (b) 1.02 THz and (c) 1.88 THz

In the absorption mode, the proposed metasurface can be considered as a common single-port system since the thickness of the bottom metal layer is greater than its skin depth in the THz band; thus, the transmittance $T(\omega)$ of the meta-structure is approximately zero [35], as illustrated in Fig. 2a. At a frequency range of 0.88 to 2.10 THz, a wide absorption spectrum with 90% efficiency is observed. To illustrate the proposed bi-functional THz meta-physical device process, we illustrate the *z*-component distributions of the electric field at the perfect absorption peaks f_1 = 1.02 THz and f_2 = 1.88 THz under normal incidence in Figs. 2b and 2c, respectively. The broadband absorption response originates from two typical graphene surface plasmon resonances [36,37]. According to the distributions of the *z*-component of the near-field electric field, the resonance at the absorption peak f_1 = 1.02 THz is due to the antibonding resonance mode with higher energy bondage, and the resonance mode at the absorption peak f_2 = 1.88 THz is mainly derived from the bonding resonance mode. In general, the connection between nearby cells and the synergy between magnetic resonance and electric dipolar resonance leads to flawless broadband absorption in the THz domain. Because the suggested graphene ring is a symmetric structure, the absorption spectrum of TE polarization is identical to that of TM polarization [17].

When the opening angle $A = 0°$, the impedance matching theory is commonly applied to better describe the physical mechanism of the proposed metasurface broadband absorption response. In the broadband absorption frequency range of 1.02–1.88 THz, the relative impedance of the meta-structure in the broadband absorption mode can be obtained according to the equivalent S-parameter inversion method, which is calculated as follows [38,39]:

$$z = \frac{\sqrt{(1+S_{11})^2 - S_{21}{}^2}}{\sqrt{(1-S_{11})^2 - S_{21}{}^2}}, \tag{3}$$

where z denotes the relative impedance of the metasurface, including the real and imaginary parts, and S_{11} and S_{21} denote the reflection and transmission coefficients, respectively. According to impedance matching theory, the proposed component can absorb the incident wave to the maximum extent when the real part of the relative impedance, $Re(z)$, is close to 1 and the imaginary part, $Im(z)$, is approximately 0 over a wide frequency band [40], indicating that the effective impedance of the device is matched to that of the free space [26]. To verify this hypothesis, we present Figs. 3a and 3b, which depict the real and imaginary sections of the relative impedance of the proposed design. At a bandwidth of 1.02–1.88 THz, the real portion of the relative impedance approaches 1 while the imaginary part is 0, showing that the effective impedance of the device is equal to the effective impedance of the free space in the broadband absorption region shown [41]. Therefore, the proposed design can respond to the surrounding electromagnetic environment to the greatest extent.

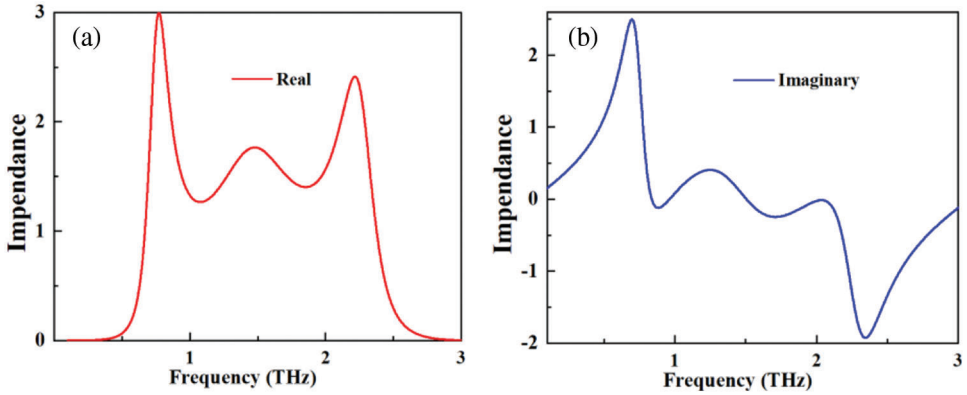

Figure 3: (a) Real and (b) Imaginary parts of the relative impedance z of the proposed design in the broadband absorption mode

The broadband absorption spectrum of graphene was estimated using simulation software. In contrast, the Fermi energy was adjusted from 0 to 0.9 eV to study the dynamic tunability of the absorption spectrum of the proposed metasurface at normal incidence, as illustrated in Fig. 4. The frequency range remains unchanged where broadband absorption occurs when the Fermi energy of graphene rises from 0 to 0.9 eV. A perfect broadband absorption response requires an amplitude increase of 20% to 100%. The change in the Fermi energy of graphene is due to the strength of its surface conductivity, which can be achieved by chemical doping or applying a bias voltage [42–45], thereby realizing the active tunable characteristics of the broadband absorption spectrum. The Fermi energy of graphene can be adjusted to obtain an amplitude modulation depth of approximately 80%. The meta-device operation may be switched between broadband absorption and reflection at will, increasing its use in terahertz transmission, as demonstrated in Fig. 4b.

In addition to examining the active tuning features, we examined the effect of structural factors on the absorption spectra when the unit-cell period p stays constant. When the outer diameter R_1 of the graphene ring was gradually increased from 13 to 17 μm, the bandwidth of the absorption spectrum gradually increased, and the peak absorption rate remained above 95%. Setting R_1 = 16 μm, the effective bandwidth with absorption efficiency above 90% reached 1.24 THz, and the relative bandwidth was 83.78%, indicating the achievement of a perfect absorption state. In addition, the absorption response at the first resonance frequency decreased with increasing R_1 because an increase in the effective width of the graphene ring weakened the attraction between the charges and thus reduced the peak absorption response [46,47], as illustrated in Fig. 5a. Fig. 5b illustrates the change in the absorption spectrum as the

inner diameter of the graphene ring changes. As R_2 increased from 3 to 7 μm, the changes in the two resonance frequencies were opposite those of increasing the outer diameter R_1. This phenomenon occurred because increasing the outer diameter could be equivalent to decreasing the inner diameter.

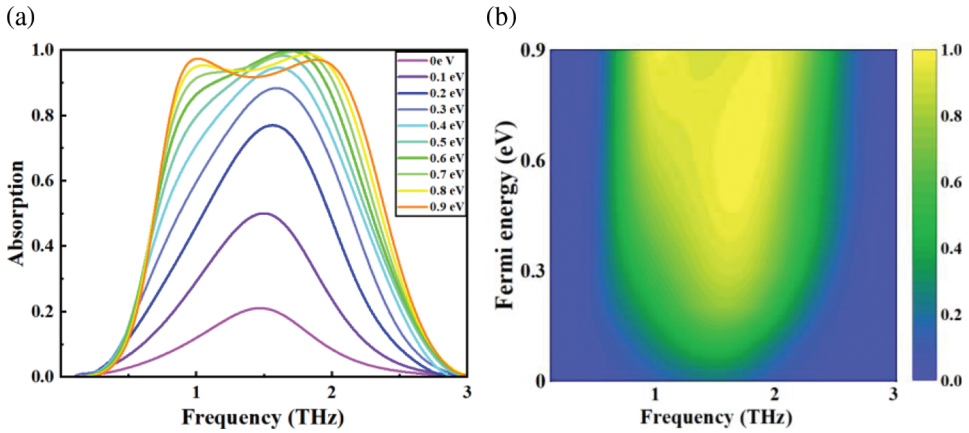

Figure 4: (a) Absorption curves and (b) Color map of the proposed design under different graphene Fermi energies

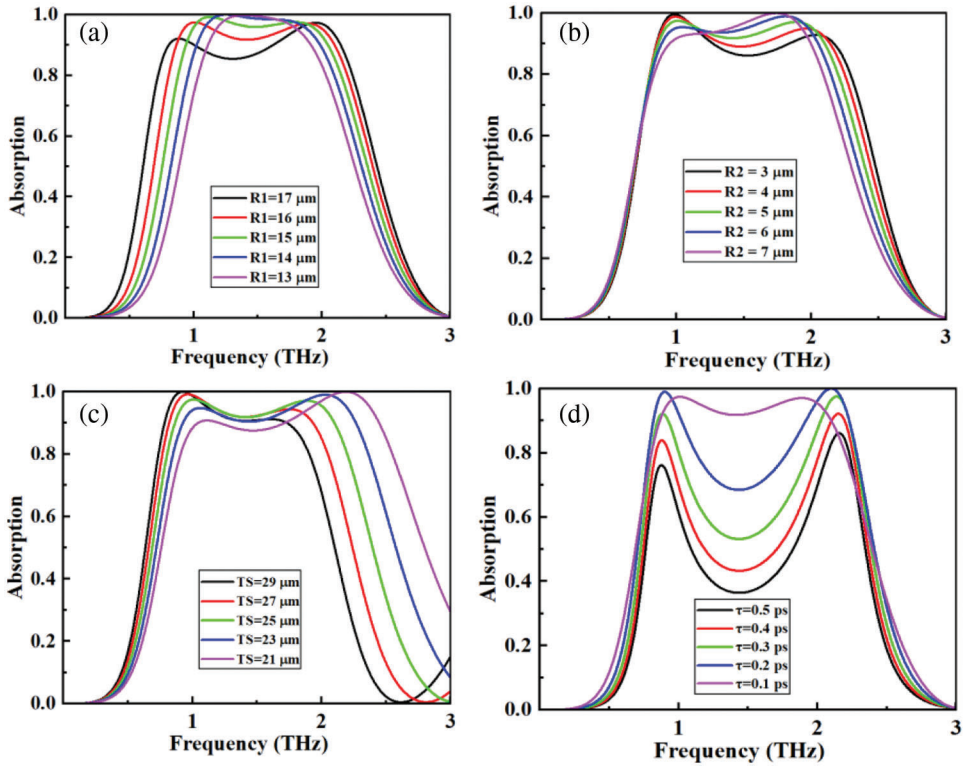

Figure 5: Absorption curves of the proposed design with different (a) Outer diameter R_1 and (b) Inter diameter R_2 of the graphene ring; (c) Thickness of the dielectric layer TS and (d) Relaxation time τ

Furthermore, as *TS* increased, the resonant frequencies of f_1 and f_2 were blue-shifted. Specifically, the frequency at f_2 moved faster than at f_1, from 2.18 to 1.60 THz; hence, the frequency range with an efficiency exceeding 80% became 1.63 to 1.16 THz, as illustrated in Fig. 5b. We also investigated the influence of the relaxation time τ of graphene on the absorption spectrum. When τ increased from 0.1 to 0.5 ps, the absorption rate at the center frequency of the absorption band decreased rapidly and gradually changed from broadband absorption to dual-band absorption, as illustrated in Fig. 5c. The main factor causing the change in τ is the doping concentration of graphene, which is related to the actual process.

In practical applications, THz waves are not perpendicularly incident on the surface of the meta-device; thus, it is necessary to investigate the broadband absorption properties of the metasurface at oblique incidence. The working bandwidth position changed slightly as the incidence angle rose from 0° to 80° when TM polarization was used. Consequently, the broadband absorption response was maintained at over 80% until the incidence angle approached 40°. As the incident angle increased, the effective contact area between the incident THz wave and the graphene split ring decreased. Therefore, the absorption rate decreased accordingly. When the incidence angle was greater than 50°, and the frequency range was focused, and the broadband absorption performance was relatively stable for the TE polarization mode, with absorption of more than 90% in the frequency range of 0.87–2.22 THz. Figs. 6c and 6d show that when the incidence angle rose over 50°, the absorption bandwidth narrowed [48].

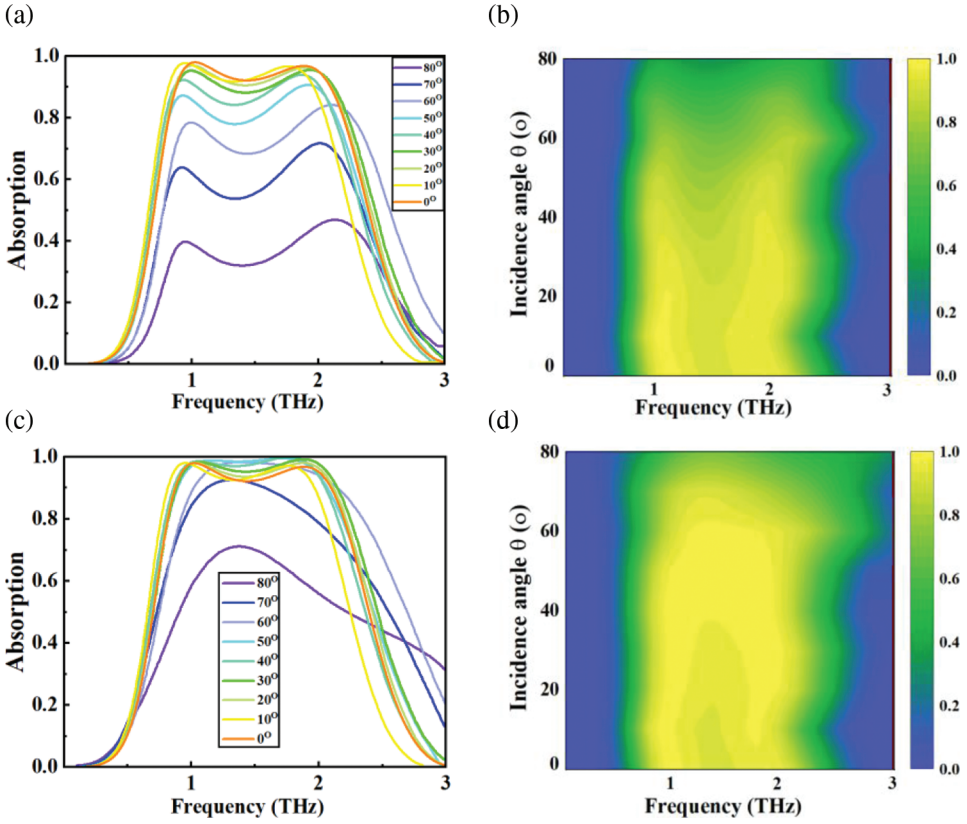

Figure 6: Absorption curves and color maps of the proposed structure with different incident angles of (a) (b) TM and (c) (d) TE polarization modes

3.2 Proposed Switchable Metasurface Behaves as a Broadband Polarization Converter When A is Fixed at 40°

The graphene ring presents a certain opening angle along the diagonal of the *xoy* plane, called a graphene split ring, and the opening angle A was fixed at 40°. According to the theory of polarization optics, the designed metasurface will behave as a linear polarization converter whose function is similar to a half-wave plate [49,50], as illustrated in Fig. 7a. Therefore, when the $x(y)$ linearly polarized wave is perpendicularly incident on the device surface, the incident wave will be converted into a $y(x)$ linearly polarized wave with orthogonal polarization. The polarization conversion effect of this meta-structure can be described by a generalized reflection matrix [19]:

$$R = \begin{pmatrix} R_{xx} & R_{xy} \\ R_{yx} & R_{yy} \end{pmatrix} \tag{4}$$

where R_{xx} and R_{yy} are the co-polarized reflection coefficients, respectively; R_{xy} and R_{yx} are the cross-polarized reflection coefficients. When the $x(y)$ polarized wave is incident vertically, the reflection coefficients are symmetric because of the symmetry of the structure; that is $R_{xx} = R_{yy}$ and $R_{xy} = R_{yx}$ [51]. For linear polarization conversion, the cross-polarization conversion rate (PCR) is calculated as follows:

$$\begin{cases} PCR_x = \dfrac{|R_{yx}|^2}{|R_{xx}|^2 + |R_{yx}|^2} \\ PCR_y = \dfrac{|R_{xy}|^2}{|R_{yy}|^2 + |R_{xy}|^2} \end{cases} \tag{5}$$

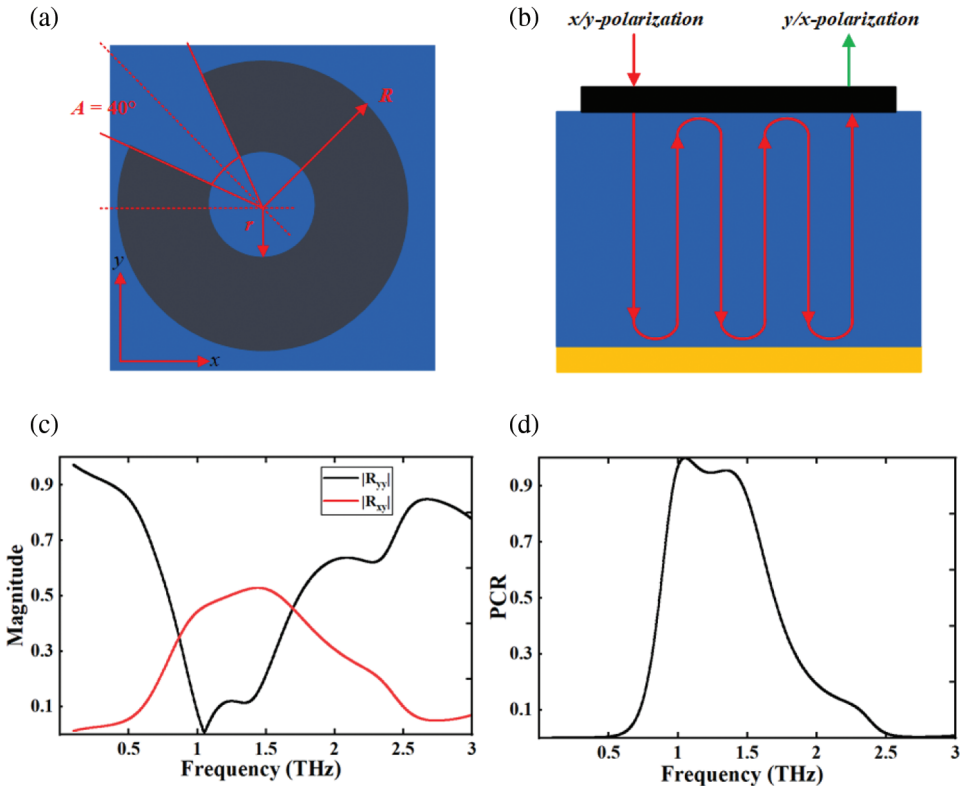

Figure 7: (a) Top view of the unit cell structure of the proposed design when the angle parameter A is fixed at 40°. (b) Schematic of the broadband polarization conversion process of a reflective metasurface. (c) Reflection coefficient and (d) PCR curve when a terahertz wave polarized along the y-axis is incident perpendicularly

The reflection coefficient and PCR curve of the proposed design are illustrated in Figs. 7c and 7d under the graphene Fermi energy of 0.7 eV. As R_{yy} was less than 0.2 and R_{xy} was greater than 0.4 for frequencies between 0.97 and 1.47 THz, the appropriate polarization conversion rate was greater than 90%. After being reflected by the metasurface, R_{yy} took the lowest value of 0.007 at the resonance frequency of 1.05 THz, which showed that the orthogonal polarization state of the y-polarized incoming wave was transformed. The calculation bandwidth of the PCR exceeding 90% reached 0.5 THz, and the frequency range was 0.97–1.47 THz. In addition, the magnitude of PCR at the peak frequency f = 1.05 THz was almost 1, which means that the incident y-linearly-polarized wave was completely converted into an x-linearly-polarized wave at this peak frequency.

We examined the active tunability of the proposed design and simulated PCR curves at different Fermi energies. When E_f decreased from 0.7 to 0.3 eV, the peak value of the broadband PCR curve first decreased and then increased, and the peak frequency blue-shifted from 1.05 to 1.38 THz. When E_f = 0.7 eV, the PCR curve showed two resonance frequency peaks, with the most noticeable broadband at 0.5 THz from 0.97 to 1.47 THz for 90% of the PCR response. In addition, when E_f = 0.4 eV, the proposed metasurface behaved as a narrow-band THz polarization converter, and the polarization conversion efficiency reached 100% at f = 1.34 THz. As E_f decreased, the PCR spectrum gradually disappeared, as shown in Fig. 8a. Therefore, the PCR operating frequency and bandwidth are dynamically tunable and may be obtained in real-world applications by introducing an external bias voltage or doping.

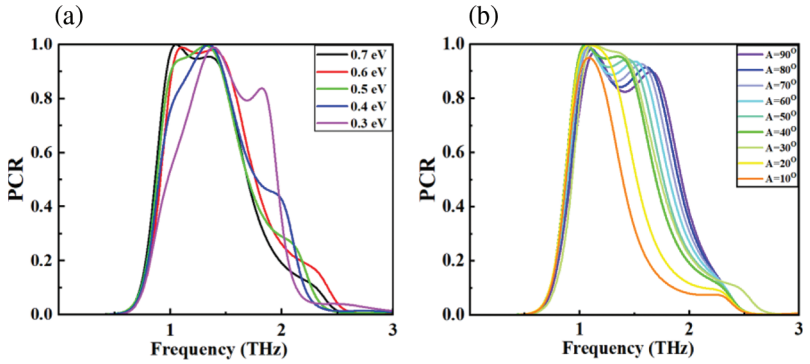

Figure 8: PCR curves with different (a) Fermi energies of graphene and (b) Opening angles As of the graphene sheet

To illustrate the characteristic parameter, that is, the influence of the change in the opening angle A on the polarization conversion efficiency, we provide Fig. 8b, which is a schematic of the polarization conversion efficiency when A is increased from 10° to 90°. The bandwidth with a PCR greater than 80% gradually increased from 0.29 to 0.76 THz. Specifically, when A = 20°, the designed metasurface exhibited single-band linear polarization conversion characteristics [52]. The PCR effect almost reached 1 at the resonance frequency peak of 1.09 THz, indicating that the y-polarized incident wave realized perfect linear polarization conversion under the reflection of the metasurface. When parameter A increased, the spectrum bandwidth gradually widened, the center frequency blue-shifted, and the corresponding PCR dropped from 0.97 to 0.82. We chose A = 40° as the optimal solution during the debugging process because the proposed metasurface had relatively flat broadband and high polarization performance here, as illustrated in Fig. 8b. The optimum opening angle can be chosen for practical applications by considering the requirements of the polarization frequency range being used.

We simulated the dependency of the proposed design of the PCR spectrum on the incidence angle, considering that the incident wave would be incident at various angles in real applications. Fig. 9 illustrates that when the electric field of the incident wave is parallel to the *x*-axis, the performance of the broadband polarization conversion had an incident range of 0°–50°, and the bandwidth of PCR sustained above 90% approached 0.41 THz. As the incidence angle grew, the bandwidth of the PCR spectrum became smaller and eventually halved when the incident angle approached 60°. The result shows that when the electric field of the incident wave is parallel to the *y*-axis, the proposed design exhibits outstanding polarization conversion performance across a wide angle of incidence range of 0° to 40°. The PCR spectrum, conversely, progressively faded away when the incidence angle increased. Asymmetry exists in the *x*- and *y*-axes on the top graphene open ring: the incident wave electric field parallel to the *x*-axis is incident in the direction close to the graphene opening, whereas the incident wave electric field parallel to the *y*-axis is incident in the direction away from the opening. Hence, the performance of polarization switching in the *x* and *y* directions of the structure differs.

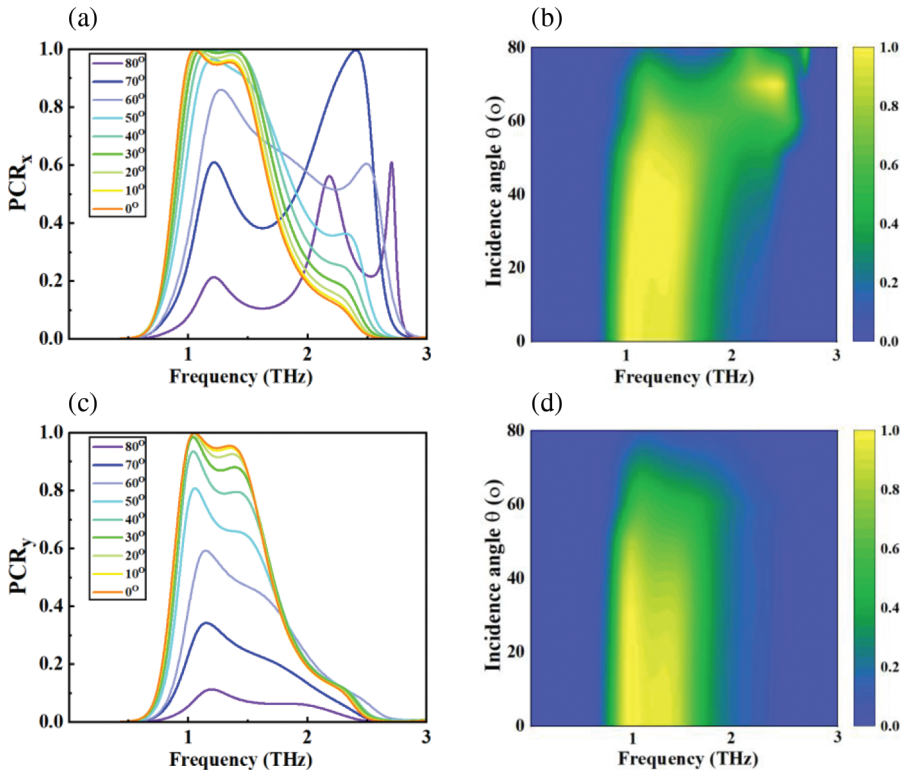

Figure 9: PCR curves and color maps of the proposed polarization converter with different incident angles of (a) *x* and (b) *y* polarization incident waves

4 Conclusion

In this work, we propose a dynamically tunable bi-functional THz device based on monolayer graphene metamaterials. The simulation analysis results show that when the opening angle of the annular graphene is fixed at 0°, the proposed metasurface behaves as a broadband absorber that can achieve a perfect broadband absorption response in the frequency range of 0.88–2.10 THz. The exact broadband absorption properties of graphene are calculated by superimposing two typical graphene surface plasmon resonance responses, and the physical process responsible for this is explained using the impedance matching theory. Conversely,

when the opening angle of the annular graphene is set at 40°, the proposed metasurface operates as a linear polarization converter. Using the equations of motion, the linear *y*-polarized wave has a bandwidth exceeding 90% of the polarization conversion efficiency when the wave is incident vertically. The frequency range is 0.97–1.47 THz, and it is completely converted to the *x*-polarized reflected wave at a frequency of 1.05 THz. Further simulations demonstrate that the proposed metasurface can dynamically adjust the frequency range and peak frequency of the electromagnetic response by manipulating the Fermi energy of graphene in two modes. In addition, both broadband absorption and linear polarization conversion spectra exhibit insensitivity to the incident angle, allowing a large incident angle within 40° under high-performance working conditions. Therefore, the proposed design has advantages such as dual functionality, high efficiency, broadband, and active tunability. Moreover, the design may have more promising applications in the THz range, such as in modulators, sensors, stealth, and optoelectronic switches. THz wave polarization and beam control also have broad application prospects in the field of intelligent systems. The designed metasurface has many working performance advantages; in material selection, graphene–carbon-based nanomaterials obtained as metamaterials from renewable resources are suitable for future large-scale production due to their advantages of environmental protection, sustainability, developability, and high economic benefits.

Funding Statement: This research was supported by the High Level Talent Project of Basic and Applied Basic Research (Natural Science) of Hainan Province in 2019 (No. 2019RC158); and by the Project of the Education Department of Hainan Province (No. Hnky2020ZD-2), all support is gratefully acknowledged.

Conflicts of Interest: The authors declare that they have no conflicts of interest to report regarding the present study.

References

1. Tonouchi, M. (2007). Cutting-edge terahertz technology. *Nature Photonics, 1(2),* 97–105. DOI 10.1038/nphoton.2007.3.
2. Ferguson, B., Zhang, X. C. (2002). Materials for terahertz science and technology. *Nature Materials, 1(1),* 26–33. DOI 10.1038/nmat708.
3. Xie, X., Rong, B., Kadoch, M. (2021). Explaining 6G Spectrum THz, mmWave, Sub 6, and Low-Band. *6G Wireless Communications and Mobile Networking,* 1–22. DOI 10.2174/9781681087962121010l.
4. Bessou, M., Chassagne, B., Caumes, J. P., Pradère, C., Maire, P. et al. (2012). Three-dimensional terahertz computed tomography of human bones. *Applied Optics, 51(28),* 6738–6744. DOI 10.1364/AO.51.006738.
5. Wang, S., Zhang, X. C. (2004). Pulsed terahertz tomography. *Journal of Physics D: Applied Physics, 37(4),* R1–R36. DOI 10.1088/0022-3727/37/4/R01.
6. Federici, J. F., Schulkin, B., Huang, F., Gary, D., Barat, R. et al. (2005). THz imaging and sensing for security applications—explosives, weapons and drugs. *Semiconductor Science and Technology, 20(7),* S266–S280. DOI 10.1088/0268-1242/20/7/018.
7. Liu, H. B., Zhong, H., Karpowicz, N., Chen, Y., Zhang, X. C. (2007). Terahertz spectroscopy and imaging for defense and security applications. *Proceedings of the IEEE, 95(8),* 1514–1527. DOI 10.1109/JPROC.2007.898903.
8. Chen, H. T., Padilla, W. J., Zide, J. M., Gossard, A. C., Taylor, A. J. et al. (2006). Active terahertz metamaterial devices. *Nature, 444(7119),* 597–600. DOI 10.1038/nature05343.
9. Holloway, C. L., Kuester, E. F., Gordon, J. A. (2012). An overview of the theory and applications of metasurfaces: The two-dimensional equivalents of metamaterials. *IEEE Antennas and Propagation Magazine, 54(2),* 10–35. DOI 10.1109/MAP.2012.6230714.
10. Tretyakov, S. A. (2015). Metasurfaces for general transformations of electromagnetic fields. *Philosophical Transactions of the Royal Society A: Mathematical, Physical and Engineering Sciences, 373(2049),* 20140362. DOI 10.1098/rsta.2014.0362.

11. Zhang, W., Zhang, L., Wu, X. (2020). Design of low-profile wide-band high-gain circularly polarized antenna based on metasurface. *2020 IEEE MTT-S International Conference on Numerical Electromagnetic and Multiphysics Modeling and Optimization (NEMO)*, pp. 1–3. Hangzhou, China, IEEE.
12. Huo, P., Zhang, S., Liang, Y., Lu, Y., Xu, T. (2019). Hyperbolic metamaterials and metasurfaces: Fundamentals and applications. *Advanced Optical Materials, 7(14),* 1801616. DOI 10.1002/adom.201801616.
13. Yu, Y., Sun, B. (2018). Terahertz absorber based on Fano-like resonance of inverted quadrangular frustum pyramid metal grooves and sensor application. *Journal of Optics, 20(7),* 075104. DOI 10.1088/2040-8986/aac842.
14. Liu, W., Song, Z., Wang, W. (2021). A high-performance broadband terahertz absorber based on multilayer graphene squares. *Physica Scripta, 96(5),* 055504. DOI 10.1088/1402-4896/abe74f.
15. Alves, F., Kearney, B., Grbovic, D., Lavrik, N. V., Karunasiri, G. (2012). Strong terahertz absorption using SiO2/Al based metamaterial structures. *Applied Physics Letters, 100(11),* 111104. DOI 10.1063/1.3693407.
16. Kang, W., Gao, Q., Dai, L., Zhang, Y., Zhang, H. et al. (2020). Dual-controlled tunable terahertz coherent perfect absorption using Dirac semimetal and vanadium dioxide. *Results in Physics, 19(1),* 103688. DOI 10.1016/j.rinp.2020.103688.
17. Hu, D., Meng, T., Wang, H., Ma, Y. (2020). Tunable broadband terahertz absorber based on plasmon hybridization in monolayer graphene ring arrays. *Applied Optics, 59(35),* 11053–11058. DOI 10.1364/AO.409738.
18. Sun, W., He, Q., Hao, J., Zhou, L. (2011). A transparent metamaterial to manipulate electromagnetic wave polarizations. *Optics Letters, 36(6),* 927–929. DOI 10.1364/OL.36.000927.
19. Yadav, V. S., Ghosh, S. K., Bhattacharyya, S., Das, S. (2018). Graphene-based metasurface for a tunable broadband terahertz cross-polarization converter over a wide angle of incidence. *Applied Optics, 57(29),* 8720–8726. DOI 10.1364/AO.57.008720.
20. Yang, X., Zhang, B., Shen, J. (2018). An ultra-broadband and highly-efficient tunable terahertz polarization converter based on composite metamaterial. *Optical and Quantum Electronics, 50(8),* 1–11. DOI 10.1007/s11082-018-1571-4.
21. Zhang, J., Zhang, K., Cao, A., Liu, Y., Kong, W. (2020). Bi-functional switchable broadband terahertz polarization converter based on a hybrid graphene-metal metasurface. *Optics Express, 28(18),* 26102–26110. DOI 10.1364/OE.397338.
22. Xu, Z., Sheng, H., Wang, Q., Zhou, L., Shen, Y. (2021). Terahertz broadband polarization converter based on the double-split ring resonator metasurface. *SN Applied Sciences, 3(9),* 1–7. DOI 10.1007/s42452-021-04751-w.
23. Li, X., Tang, S., Ding, F., Zhong, S., Yang, Y. et al. (2019). Switchable multifunctional terahertz metasurfaces employing vanadium dioxide. *Scientific Reports, 9(1),* 1–13. DOI 10.1038/s41598-019-41915-6.
24. Shabanpour, J., Beyraghi, S., Cheldavi, A. (2020). Ultrafast reprogrammable multifunctional vanadium-dioxide-assisted metasurface for dynamic THz wavefront engineering. *Scientific Reports, 10(1),* 1–14. DOI 10.1038/s41598-020-65533-9.
25. Liu, S., Cui, T. J., Xu, Q. (2016). Anisotropic coding metamaterials and their powerful manipulation of differently polarized terahertz waves. *Light: Science & Applications, 5(5),* e16076. DOI 10.1038/lsa.2016.76.
26. Kumar, P., Lakhtakia, A., Jain, P. K. (2019). Graphene pixel-based polarization-insensitive metasurface for almost perfect and wideband terahertz absorption. *Journal of the Optical Society of America B, 36(8),* F84–F88. DOI 10.1364/JOSAB.36.000F84.
27. Torres, F. G., Troncoso, O. P., Rodriguez, L., De-la-Torre, G. E. (2021). Sustainable synthesis, reduction and applications of graphene obtained from renewable resources. *Sustainable Materials and Technologies, 29,* e00310. DOI 10.1016/j.susmat.2021.e00310.
28. Xu, J., Wang, S., Yang, C., Li, T., Liu, Q. et al. (2021). Free-standing two-dimensional ruthenium-beryllium nanosheets for alkaline hydrogen evolution. *Chemical Engineering Journal, 421,* 129741. DOI 10.1016/j.cej.2021.129741.
29. Xu, J., Kong, X. (2022). Amorphous/crystalline heterophase ruthenium nanosheets for pH-universal hydrogen evolution. *Small Methods, 6(3),* 2101432. DOI 10.1002/smtd.202101432.
30. Xiong, H., Ji, Q., Bashir, T., Yang, F. (2020). Dual-controlled broadband terahertz absorber based on graphene and Dirac semimetal. *Optics Express, 28(9),* 13884–13894. DOI 10.1364/OE.392380.
31. Hanson, G. W. (2008). Dyadic green's functions and guided surface waves for a surface conductivity model of graphene. *Journal of Applied Physics, 103(6),* 064302. DOI 10.1063/1.2891452.

32. Li, Q., Zhu, J., Wang, S., Huang, F., Liu, Q. et al. (2020). Microwave absorption on a bare biomass derived holey silica-hybridized carbon absorbent. *Carbon, 161,* 639–646. DOI 10.1016/j.carbon.2020.01.087.
33. Li, Q., Li, S., Liu, Q., Liu, X., Shui, J. et al. (2021). Iodine cation bridged graphene sheets with strengthened interface combination for electromagnetic wave absorption. *Carbon, 183,* 100–107. DOI 10.1016/j.carbon. 2021.07.015.
34. Chen, L., Song, Z. (2020). Simultaneous realizations of absorber and transparent conducting metal in a single metamaterial. *Optics Express, 28(5),* 6565–6571. DOI 10.1364/OE.388066.
35. Wu, G., Jiao, X., Wang, Y., Zhao, Z., Wang, Y. et al. (2021). Ultra-wideband tunable metamaterial perfect absorber based on vanadium dioxide. *Optics Express, 29(2),* 2703–2711. DOI 10.1364/OE.416227.
36. Prodan, E., Radloff, C., Halas, N. J., Nordlander, P. (2003). A hybridization model for the plasmon response of complex nanostructures. *Science, 302(5644),* 419–422. DOI 10.1126/science.1089171.
37. Mou, N., Sun, S., Dong, H., Dong, S., He, Q. et al. (2018). Hybridization-induced broadband terahertz wave absorption with graphene metasurfaces. *Optics Express, 26(9),* 11728–11736. DOI 10.1364/OE.26.011728.
38. Ding, F., Dai, J., Chen, Y., Zhu, J., Jin, Y. et al. (2016). Broadband near-infrared metamaterial absorbers utilizing highly lossy metals. *Scientific Reports, 6(1),* 1–9. DOI 10.1038/srep39445.
39. Huang, J., Li, J., Yang, Y., Li, J., Zhang, Y. et al. (2020). Active controllable dual broadband terahertz absorber based on hybrid metamaterials with vanadium dioxide. *Optics Express, 28(5),* 7018–7027. DOI 10.1364/OE.387156.
40. Cheng, Y. Z., Fang, C., Zhang, Z., Wang, B., Chen, J. et al. (2016). A compact and polarization-insensitive perfect metamaterial absorber for electromagnetic energy harvesting application. *Progress in Electromagnetic Research Symposium (PIERS)*, pp. 1910–1914. Shanghai, China, IEEE.
41. Lv, F., Xiao, Z., Lu, X., Chen, M. (2020). Three-dimensional ultra-broadband metamaterial absorber with full graphite structure. *Journal of Electronic Materials, 49(1),* 689–694. DOI 10.1007/s11664-019-07735-0.
42. Song, Y., Xie, Z., Ma, Y., Li, Z. L., Wang, C. K. (2014). Giant rectification ratios of azulene-like dipole molecular junctions induced by chemical doping in armchair-edged graphene nanoribbon electrodes. *Journal of Physical Chemistry C, 118(32),* 18713–18720. DOI 10.1021/jp504448n.
43. Liu, H., Liu, Y., Zhu, D. (2011). Chemical doping of graphene. *Journal of Materials Chemistry, 21(10),* 3335–3345. DOI 10.1039/C0JM02922J.
44. Das, A., Pisana, S., Chakraborty, B., Piscanec, S., Saha, S. K. et al. (2008). Monitoring dopants by Raman scattering in an electrochemically top-gated graphene transistor. *Nature Nanotechnology, 3(4),* 210–215. DOI 10.1038/nnano.2008.67.
45. Chen, C. F., Park, C. H., Boudouris, B. W., Horng, J., Geng, B. et al. (2011). Controlling inelastic light scattering quantum pathways in graphene. *Nature, 471(7340),* 617–620. DOI 10.1038/nature09866.
46. Le, K. Q., Bai, J. (2015). Enhanced absorption efficiency of ultrathin metamaterial solar absorbers by plasmonic Fano resonance. *Journal of the Optical Society of America B, 32(4),* 595–600. DOI 10.1364/JOSAB.32.000595.
47. Wang, B. X., Wang, L. L., Wang, G. Z., Huang, W. Q., Li, X. F. et al. (2014). A simple design of a broadband, polarization-insensitive, and low-conductivity alloy metamaterial absorber. *Applied Physics Express, 7(8),* 082601. DOI 10.7567/APEX.7.082601.
48. Li, Z., Yang, R., Wang, J., Zhao, Y., Tian, J. et al. (2021). Multifunctional metasurface for broadband absorption, linear and circular polarization conversions. *Optical Materials Express, 11(10),* 3507–3519. DOI 10.1364/OME.437474.
49. Ding, F., Wang, Z., He, S., Shalaev, V. M., Kildishev, A. V. (2015). Broadband high-efficiency half-wave plate: A supercell-based plasmonic metasurface approach. *ACS Nano, 9(4),* 4111–4119. DOI 10.1021/acsnano.5b00218.
50. Xia, R., Jing, X., Gui, X., Tian, Y., Hong, Z. (2017). Broadband terahertz half-wave plate based on anisotropic polarization conversion metamaterials. *Optical Materials Express, 7(3),* 977–988. DOI 10.1364/OME.7.000977.
51. Tahir, F. A. (2019). A Broadband metasurface for cross polarization conversion applications. *IEEE International Conference on Computational Electromagnetics (ICCEM)*, pp. 1–2. Shanghai, China, IEEE.
52. Liao, K., Liu, S., Zheng, X., Zhang, X., Shao, X. et al. (2021). A polarization converter with single-band linear-to-linear and dual-band linear-to-circular based on single-layer reflective metasurface. *International Journal of RF and Microwave Computer-Aided Engineering, 32(2),* e22955.